Electronic essential states model applied to squaraine molecular crystals

Robert Schwarzl

March-June 2023

This report is the result of Robert Schwarzl's research internship at Prof. Frank Spano at the Temple University in Philadelphia, PA, USA. Collaborators are Assoc.Prof. Markus Koch and Maximilan Jeindl at Graz University of Technology, Prof. Frank Spano at Temple University in Philadelphia, apl.Prof. Manuela Schiek at Johannes Kepler University Linz and National Metrology Institute in Braunschweig, Davide Giavazzi and Prof. Anna Painelli at the University of Parma and Andreas Windischbacher and Prof. Peter Puschnig at the University of Graz.

While the topic of organic molecular aggregates is at the border between physical and organic chemistry, molecular and computational physics, a lot of this publication is focussed on computer science-related problems. This is because writing reusable, extensible, documented, modern and readable code with good performance necessary for tackling larger systems was a key aspect of the research internship. The complete code described here will be published once a satisfactory level is reached and is available upon reasonable request until then.

Contents

1. Introduction to squaraines

Organic semiconductors have been in active research for many decades. Among biosensors, fluorescence markers and organic photovoltaic cells, organic light emitting diodes have likely reached the most widespread use beyond research laboratories, being integrated into televisions, internet-of-things devices (IoT) and smartphones. It is therefore not surprising that, even today, new compounds are investigated to extend the range of possible applications, to improve material properties and to better understand the fundamental principles governing the behavior on a molecular level. The material class under investigation, squaraines, is based on a central squaric acid moiety surrounded by aniline rings where various side chains can be attached as described in ref. [1].
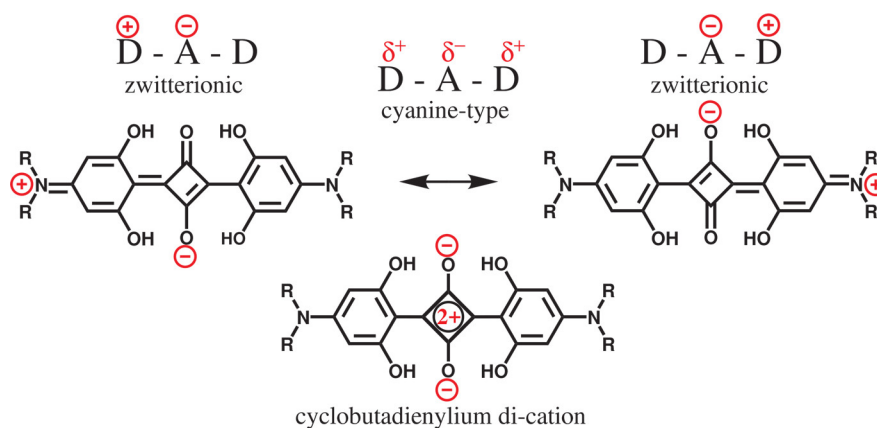

Figure 1: Zwitterionic chemical structure of anilino squaraines, ref [1]

Anilino squaraines (sec. 1) are particularly interesting because they enable the growth of multiple polymorphs by modifying the side chains and thereby altering the molecular stacking. Similar to solvatochromism, the following change in spectral properties cor-

responds to a very strong intermolecular coupling as becomes visible by comparing the spectra of isolated squaraines in a PMMA matrix [20] and the orthorhombic polymorph investigated in this publication. A thorough investigation of all processes happening after photoexcitation necessitates a theoretical model that covers the interacting molecules. In particular, the essential states model discussed in this publication is capable of simulating higher excited states by allowing multiple monomers to be excited at the same time. This is in contrast to the Kasha model where only single excitations are simulated. As the transient absorption microscope (TAM) of the Koch group in Graz [13] is capable of observing higher excitations which are not single photon allowed from the ground state via 2-photon absorption (2PA) and excited state absorption (ESA), a polarization-resolved simulation technique for higher excitations is a quintessential counterpart for experimental results.

In parallel aggregates of organic chromophores, the total intermolecular interaction can be attractive or repulsive, resulting in a red-shifted absorption peak and superluminescence (J aggregate) or blue-shifted absorption peak and suppressed photoluminescence (H aggregate) of the excited states with respect to the monomer transitions [6]. In elaborate theories involving vibronic transitions (combinations of electronic and vibrational transitions), such as a Frenkel-Holstein Hamiltonian, H and J aggregates are better characterized by the ratio of the first vibronic peaks 0-0 and 0-1. Cases of non-parallel, identical monomers can induce both J and H peaks to occur, resulting in a phenomenon called *Davydov splitting* of a single exciton into two peaks of mutually orthogonal transition dipole moment. According to polarization-resolved spectroscopic results, this Davydov splitting is particularly large in the aggregate investigated in this publication. The upper Davydov band at $1.91\,\mathrm{eV}$ is $0.23\,\mathrm{eV}$ higher or $90\,\mathrm{nm}$ lower than the lower Davydov band at $1.68\,\mathrm{eV}$ [1]. This large splitting, as well as the polarization sensitivity, are advantageous to femtosecond transient absorption experiments where the laser pulses are spectrally broader than $10\,\mathrm{nm}$ due to the Heisenberg uncertainty principle. Additionally to polarization-resolved measurements, ellipsometry results indicate two states contributing to the lower Davydov band, see ref. [3]. It is expected that a strong intermolecular coupling also corresponds to a high rate of energy transfer as observed in preliminary experimental measurements. Also, the crystalline nature of the material allows different radiationless decay pathways such as energy transfer to lattice phonons, resulting in short excited state lifetimes and the strict necessity of femtosecond spectroscopy to investigate higher excitations (see fig. 4.)

Semi-empirical models such as the Kasha model, the Frenkel-Holstein Hamiltonian and the essential states model are well established in systems of different organic semiconductors. [6] Our system of interest grows in an orthorhombic lattice with four non-parallel monomers per unit cell [1] and is, therefore, theoretically allowed to exhibit more than two split states. One reason for working with the essential states model is that there are already recent results published on similar squaraines [21, 6]. The first goal therefore is to extend the system from 2 to 4 interacting monomers, essentially forming a tetramer in the gas phase. Naturally, the choice of these four monomers is not unique as integer linear combinations of the lattice vectors can be added to each of them.

2. Motivation: Experimental results

Fig. 2 shows a transient absorption microscope capable of performing femtosecond spectroscopy on solid samples. Both light sources can be independently tuned from 650 nm to 950 nm and 500 nm to 950 nm. Due to the medium repetition rate of 40 kHz of the Light Conversion PHAROS laser, efficient second harmonics generation allows the extension of pump and probe ranges into the ultraviolet range (325 nm and 250 nm, respectively.) This and the option of inserting polarizing optics such as filters and retardation plates into the pump and probe paths makes it possible to investigate the polarization-resolved behavior of single and higher excited states on a spatial, temporal and wavelength-resolved scale. Characterization measurements indicate a spatial resolution of 3 µm, a temporal resolution of 80 fs and spectral widths of approximately 10 nm to 40 nm depending on the central wavelength. The quantity measured is called *transient absorbance* and is related to α in the Beer-Lambert law:

$$\Delta A = -\log_{10} \frac{I_\text{pump-probe}}{I_\text{probe only}} \tag{1}$$

ΔA, given in transient change of optical magnitude ΔOD, indicates a transient increase in opacity for positive values which is attributed to excited state absorption unless caused by cross-correlation effects of pump and probe. This means that the probability of absorption by causing a second excitation from an already excited state exceeds other effects. Neglecting cross-correlation effects when there is temporal overlap between the pulses, negative values (a more transparent sample) indicate ground state depletion and/or stimulated emission. Since ground state depletion occurs when a previous excitation removed part of the ground-state population, it always occurs if the probe pulse is resonant with a single excitation until all of the population fully decays back into the ground state, making it the process with the longest lifetime in this resonant case. Transient absorption microscopy, including possible processes, is explained in detail in ref. [22].

In order to motivate the choice of model, preliminary results from excited state absorption experiments are reported here. As is also visible from the Jablonski diagram in fig. 3, both the upper Davydov component UDC at 1.91 eV and the lower Davydov component LDC at 1.68 eV have transitions to higher excitations at 2.34 eV and 2.21 eV for light polarized along the upper Davydov component, correspondingly. It should be noted that the growth direction (110) of the orthorhombic samples means that the components LDC1 and LDC2 can not be excited independently as both the a and b directions always have the same projection with respect to the beam polarization. It is expected, but still investigated at the time of this work, that higher excitations also exhibit Davydov splitting. Two results from theoretical simulations are also included: (1) a linearly fitted dark state from the essential states model shown in fig. 10 at 1.79 eV and (2) a second possible dark state produced by the periodic Kasha model at 2.34 eV as shown in ref. [5].

Fig. 4 shows the underlying experimental data from the author's Master thesis [12]. While population analysis by fitting exponential functions is difficult for many of these
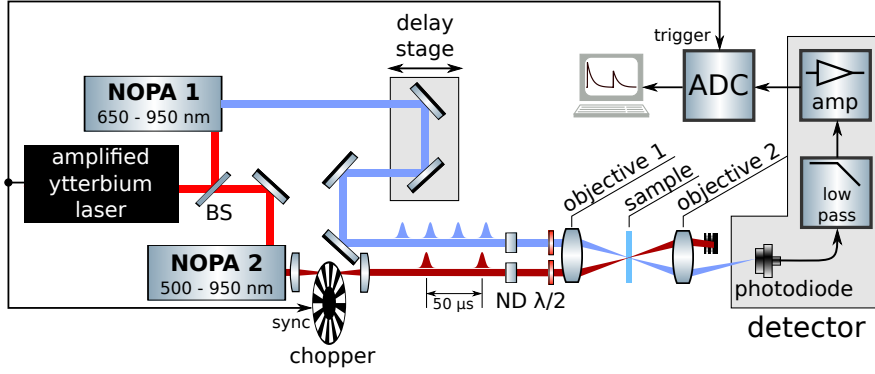
Figure 2: Transient absorption microscope used by the Koch group at TU Graz [13]. Two nonconlinear optic parametrical amplifiers (NOPAs) act as independently tuneable light sources for pump and probe. A chopper is used to block every odd pump pulse to compare the transmission of the previously excited sample with one in its electronic ground state. The result is recorded on a PicoScope and evaluated on a PC.

small contrast levels, the direction of the rising (falling) edge indicates if the sample becomes more opaque (transparent) upon photoexcitation by the pump pulse. This behavior changes at 530 nm central wavelength from pumping the upper Davydov component UDC and 560 nm central wavelength from pumping the lower Davydov component. This result is reflected in the Jablonski figure 3 under two conditions: (1) it is assumed that there is little population transfer to lower-energy states before ESA which would decrease the total energy of the higher excitations and (2) that the exact spectral position of the higher excited states is not readily available due to the presence of underlying ground state depletion (GSD) signals. Better characterization of higher excited states and an extension into the UV-B and UV-C ranges is ongoing work at the Transient Absorption Microscope in Graz at the time of writing this publication.
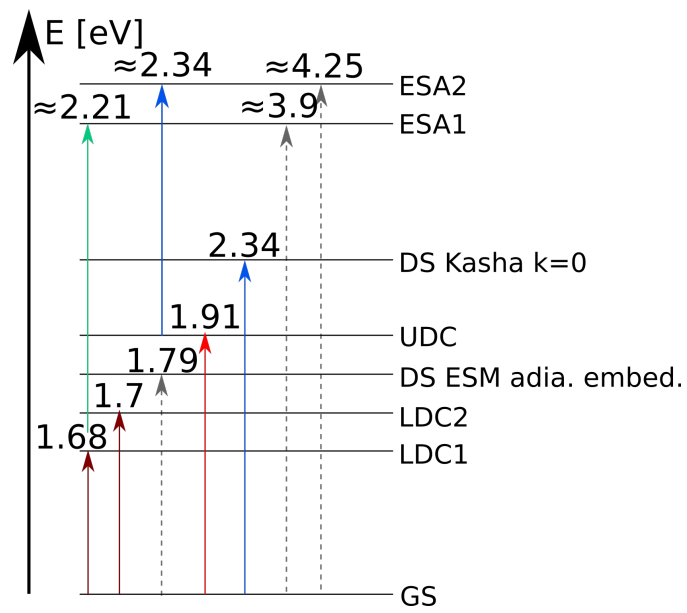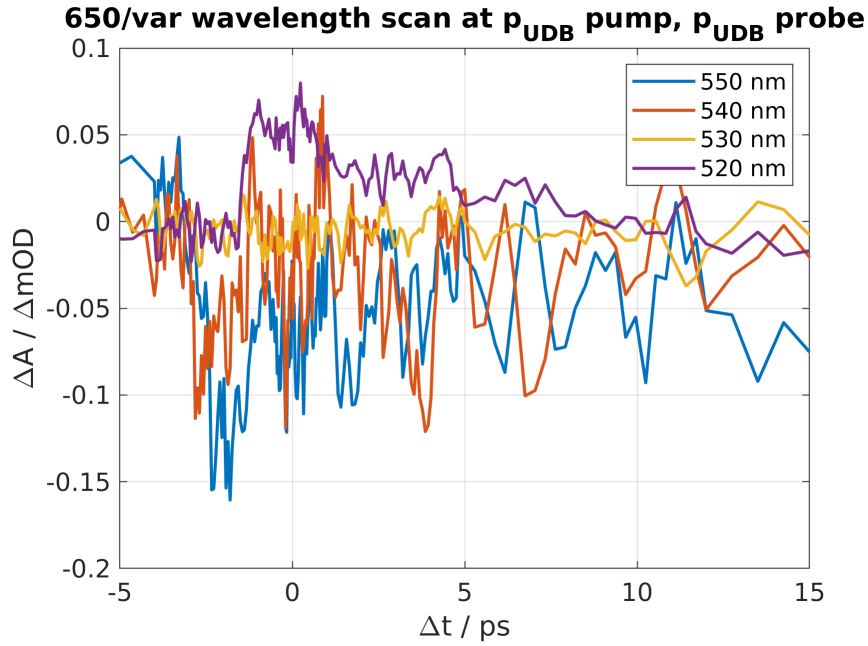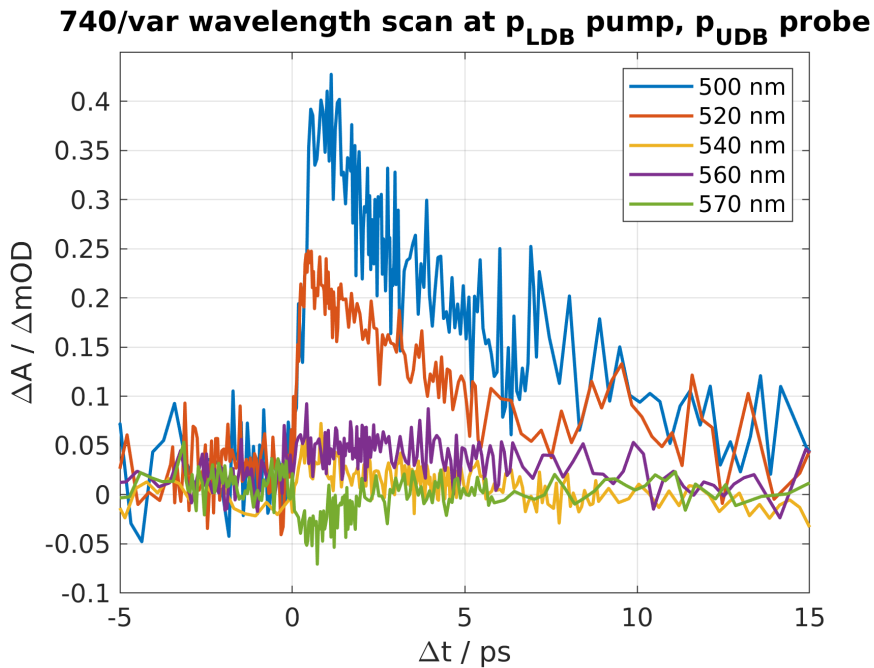
Figure 3: Jablonski diagram from experiments and some of the ESM and Kasha model results. ESA1 can be further excited from UDC by probing with energies with at least 2.34 eV and polarization along the unit cell axis c, ESA2 from the LDC1 by probing with energies of at least 2.21 eV and UDB polarization.

(a) Upper Davydov component excitation: ESA transition at 530 nm

(b) Lower Davydov component 1 excitation: ESA transition at 560 nm

Figure 4: Transient absorption delay scan results showing the appearance of excited state absorption (ESA) transitions. The transient absorptivity ΔA indicates how much more opaque a sample becomes upon photoexcitation. It can be seen that higher excitations become dominant at 530 nm=2.34 eV for UDC pump and 560 nm=2.21 eV for LDC pump.

3. Programming

Prof. Spano's code, which was used in ref. [21], is written in Fortran 77 using the ISML library for linear algebra calculations. Different versions of Fortran are widely used in the field of theoretical chemistry due to their high execution speed, their integrated syntax for complex and multidimensional arrays and available libraries for scientific and high-performance computing. However, the absence of array-wise functions and the limitations of original Fortran compilers led to the choice of the more modern Python 3 programming language [11]. To facilitate fast and accurate numerical calculations, NumPy [4], SciPy [19], CuPy [9] and SymPy [8] are used and rapid plotting is realized using the 2D and 3D interfaces of matplotlib. All matrices are set up using object-oriented Python code and functional programming. These choices are motivated by numerous considerations:

- Python and numpy have a wide variety of fast array-/matrix-wise operations which reduce the potential for programming mistakes.

- Object-oriented programming allows an inherited class structure, allowing the inclusion of additional effects such as the embedding in a mean-field crystal environment by overriding Coulomb interaction calculations.

- Lambda expressions and function pointers, two techniques often applied in functional programming, reduce the number of nested loops in the code for interaction calculations and avoid writing duplicate code. A potential downside is the increase in run time due to the increased use of the stack when compared to simple for loops.

- Python is available on all modern operating systems, particularly including Windows and Linux. It provides versatile packages for argument parsing (`argparse`), data storage (`JSON`, MATLAB data support, potentially `HDF5` and `netlib`)

- matplotlib provides interactive graphical user interfaces (GUI) for plotting.

The code is set up in a git repository to keep track of all changes and developed in the Visual Studio Code IDE for syntax highlighting, code completion, versatile debugging functions and its ease-of-use. Interactive interfaces can be coded using Jupyter notebooks.

3.1. Computational limits

While the essential states model is adequate for squaraines and accurately involves the calculation of multiple excitations, its major downside is the steep increase in computing power needed for larger systems and effects such as vibrational transitions and intermolecular charge transfer. As an example, the typical size for a tetramer is the diagonalization of a $3^4 = 81 \times 81$ matrix which can be done in milliseconds. However, including a single vibrational excitation per monomer with a maximum of five quanta of a harmonic oscillator drives this number to $(3 * 5)^4 = 50625$ basis states and memory

requirements of a few GB in dense matrix storage. Explicitly treating a 3x3x3 supercell to approximate periodic behavior increases the size to $3^{27} \approx 7.6 \times 10^{12}$ which is impossible to store in the memory or to solve in a useful run-time. It is therefore clear that the system size and the number of effects that can be considered are severely limited and that approximate solutions, such as embedding into a mean-field environment outlined in sec. 4.4, are necessary.

4. Essential States Model

The essential states model was originally devised by Anna Painelli and co-workers [17, 15, 14]. In its most basic form for calculating a D-A-D monomer, two parameters η and t are fit from optical spectroscopy experiments or an *ab-initio* calculation of a the monomer spectra. A neutral basis state $|N\rangle = DAD$ with energy 0 is coupled to two diabatic basis states $|Z_1\rangle$ and $|Z_2\rangle$, each with energy η, via the coupling constant t. The model assumes that these constants contain all intramolecular couplings within the D-A-D monomer. This results in the following Hamiltonian of *diabatic* states:

$$
\hat{H}_{\mathrm{monomer}} =
\begin{array}{c}
 \\
|N\rangle \\
|Z_1\rangle \\
|Z_2\rangle
\end{array}
\begin{array}{c}
\begin{array}{ccc}
|N\rangle & |Z_1\rangle & |Z_2\rangle
\end{array} \\
\left(
\begin{array}{ccc}
0 & t & t \\
t & \eta & 0 \\
t & 0 & \eta
\end{array}
\right)
\end{array}
\tag{2}
$$

Diagonalizing this matrix, in other words, finding the physical *adiabatic* transitions of the model, results in three different states $|g\rangle$, $|c\rangle$ and $|e\rangle$ [16]. Since the $g \to c$ transition is one-photon allowed and $g \to e$ is two-photon allowed, a knowledge of the monomer one- and two-photon absorption peaks from experiment or *ab-initio* calculations allows an exact determination of the constants η and t by solving a linear system of euqations. These results can then be used to form molecular aggregates based on physical information. In case of this orthorhombic iso-butyl squaraine (SQIB), the information is readily available from XRD [1].

The one-photon cross section from the ground state is proportional to the square of the transition dipole moment or oscillator strength μ_{t} [18]:

$$
\vec{A} \propto |\vec{\mu}_{\mathrm{l,adiabatic}}|^2
\tag{3}
$$

$$
\vec{\mu}_{\mathrm{k,diabatic}} = \sum_{ij} q_i \Delta \vec{r}_i
\tag{4}
$$

$$
\vec{\mu}_{\mathrm{l,adiabatic}} = \sum_k \vec{\mu}_{\mathrm{k,diabatic}} x_{0,k} x_{l,k}
\tag{5}
$$

where $\vec{\mu}_{\mathrm{l,adiabatic}}$ is a transition dipole moment of transition l, $\vec{\mu}_{\mathrm{k,diabatic}}$ is the sum of dipole moments of the monomers $q\Delta\vec{r}$ in diabatic state k, i is the charge center index of a tetramer (1-12 for four D-A-D chromophores), $x_{0,k}$ is the ground state eigenvector and $x_{l,k}$ is the excited state eigenvector of the desired transition l.

To calculate absorption spectra for arbitrary polarizations along the growth plane (110) [1], the following equations are used with the unit vector p and the angle between the crystal directions [1 -1 0] and [0 0 1]:

$$A(\vec{r}) = (\vec{\mu}_{\text{adiabatic}} \cdot \vec{p})^2 \tag{6}$$

$$\vec{p}(\alpha) = \begin{pmatrix} \sin(\alpha)/\sqrt{2} \\ -\sin(\alpha)/\sqrt{2} \\ \cos(\alpha) \end{pmatrix} \tag{7}$$

4.1. Dimer Hamiltonian

Molecular aggregation in the essential states model begins with at least two molecules or monomers with a known relative geometry. The diabatic basis consists of the uncharged state $|NN\rangle$, single charge transfer excitations $|Z_1 N\rangle, |Z_2 N\rangle, |NZ_1\rangle, |NZ_2\rangle$ and double charge transfer excitation $|Z_1 Z_1\rangle, |Z_1 Z_2\rangle, |Z_2 Z_1\rangle, |Z_2 Z_2\rangle$. Coupling is enabled for exciting a single monomer, e.g. $|NZ_1\rangle \leftrightarrow |Z_2 Z_1\rangle$ while $|Z_1 N\rangle \leftrightarrow |Z_2 N\rangle$ or $|Z_1 N\rangle \leftrightarrow |NZ_1\rangle$ are not directly coupled. Intermolecular interaction is modeled by calculating Coulomb terms between two excited monomers and adding them to the corresponding diagonal terms; assume the positions $\vec{r}_{00}, \vec{r}_{01}, \vec{r}_{02}$ correspond to D_1, A and D_2 coordinates of the first monomer, $\vec{r}_{10} \dots$ correspond to the second monomer, q are the corresponding unit charges and the state is $|Z_1 Z_2\rangle$, the interaction term is:

$$V_C = \frac{1}{4\pi\epsilon} \left[\frac{q_{00}q_{11}}{|\vec{r}_{11} - \vec{r}_{00}|} + \frac{q_{00}q_{12}}{|\vec{r}_{12} - \vec{r}_{00}|} + \frac{q_{01}q_{11}}{|\vec{r}_{11} - \vec{r}_{01}|} + \frac{q_{01}q_{12}}{|\vec{r}_{12} - \vec{r}_{01}|} \right] \tag{8}$$

ϵ can be assumed to be ϵ_0 in small, gaseous systems or include a relative dielectric constant ϵ_R based on experimental results or *ab-initio* calculations. Of course, all other combinations are similar. This results in the total block Hamiltonian:

$$\hat{H}_{\text{dimer}} = \begin{array}{c} |NN\rangle \\ |Z_1 N\rangle \dots \\ |Z_1 Z_1\rangle \dots \end{array} \begin{pmatrix} 0 & t & 0 \\ t & \eta_{\text{diag}} & t_{\text{single change}} \\ 0 & t_{\text{single change}} & 2\eta_{\text{diag}} \end{pmatrix} \tag{9}$$

with column headers $|NN\rangle \quad |Z_1 N\rangle \dots \quad |Z_1 Z_1\rangle \dots$

4.2. Tetramer Hamiltonian

A consequent extension of the electronic essential states model to four monomers (*tetramer*) leads to the following basis elements:

- 1 neutral state of all monomers $|NNNN\rangle$

- 8 single excited states $|Z_1 NNN\rangle \dots |NNNZ_2\rangle$

- 24 double excited states $|Z_1 Z_1 NN\rangle \dots |NNZ_2 Z_2\rangle$

- 32 triple excited states $|Z_1 Z_1 Z_1 N\rangle \dots |NZ_2 Z_2 Z_2\rangle$

10

- 16 quadruple excited states $|Z_1 Z_1 Z_1 Z_1\rangle \ldots |Z_2 Z_2 Z_2 Z_2\rangle$

All matrix elements with a difference of a single excitation (for example $|NNZ_1N\rangle \leftrightarrow |Z_2NZ_1N\rangle$) have the same coupling strength t as in the monomer case while all other non-diagonal elements are 0 in lack of coupling. The total Hamiltonian for a tetramer in open boundary conditions is therefore:

$$\hat{H} = \begin{array}{c} \\ |NNNN\rangle \\ |Z_1NNN\rangle \ldots \\ |Z_1Z_1NN\rangle \ldots \\ |Z_1Z_1Z_1N\rangle \ldots \\ |Z_1Z_1Z_1Z_1\rangle \ldots \end{array} \begin{array}{ccccc} |NNNN\rangle & |Z_1NNN\rangle\ldots & |Z_1Z_1NN\rangle\ldots & |Z_1Z_1Z_1N\rangle\ldots & |Z_1Z_1Z_1Z_1\rangle\ldots \\ \left(\begin{array}{ccccc} 0 & t & 0 & 0 & 0 \\ t & \eta_{\text{diag}} & t_{\text{single change}} & 0 & 0 \\ 0 & t_{\text{single change}} & 2\eta_{\text{diag}} + V_C & t_{\text{single change}} & 0 \\ 0 & 0 & t_{\text{single change}} & 3\eta_{\text{diag}} + V_C & t_{\text{single change}} \\ 0 & 0 & 0 & t_{\text{single change}} & 4\eta_{\text{diag}} + V_C \end{array}\right) \end{array}$$

$$(10)$$

While the diagonalization results in 81 eigenvectors or 80 transitions ($E_{\text{excited}} - E_{\text{ground state}}$), only very few of them show a non-zero transition dipole moment from the ground state $\mu_{\text{adiabatic}} = \langle g|\hat{\mu}|e\rangle$. All of the transitions can play a role in two-photon absorption and excited state absorption (ESA) calculations, but these are beyond the scope of this work and will be investigated in the future.

4.3. Diabatic embedding

While the tetramer in section 4.2 already uses the correct arrangements of the monomers according to XRD measurements, there is not yet any interaction beyond a single unit cell. Due to computational limitations as outlined in 3.1, approximate solutions for the treatment of a periodic crystal have to be found. In its simplest case, this is done on the level of the basis set without any knowledge of the physical system:

1. The 81 diabatic states are copied to all neighboring unit cells.

2. All Coulomb interaction terms V_C are extended to include interactions with the newly added unit cells. This includes single excitations as, for example, the single excitation Z_1 in the diabatic state $|Z_1NNN\rangle$ now also interacts with the charge centers of the corresponding state in all neighboring unit cells.

As can be seen, this does not increase the basis set size from 81×81, so only the building of the Hamiltonian takes longer due to the added interaction terms. However, this also means that each of the diabatic basis states is assumed to be interacting with a different electronic configuration. Due to the lack of coupling between the diabatic states, this does not reproduce the real physical system accurately and is actually farther away from the experiment than the system with open boundary conditions. **Some nice graphics here**

4.4. Adiabatic embedding

Another approach suggested by Davide Giavazzi is similar to other mean-field theories. Here, instead of using the diabatic states to embed the explicitly treated system, the charges of neighboring unit cells assigned in a self-consistent calculation. Starting from an elementary charge matrix of the form:

$$\hat{q}_{\text{diabatic}} = \begin{pmatrix} 0 & 0 & 0 & 0 & 0 & 0 & 0 & 0 & 0 & 0 & 0 & 0 \\ 1 & -1 & 0 & 0 & 0 & 0 & 0 & 0 & 0 & 0 & 0 & 0 \\ 0 & -1 & 1 & 0 & 0 & 0 & 0 & 0 & 0 & 0 & 0 & 0 \\ & & & & & \vdots & & & & & & \end{pmatrix} \tag{11}$$

and orthonormal eigenvectors $\vec{x}_i$ from the diagonalization of previous calculations, the charges can be calculated by base transformation:

$$\vec{q}_{\text{i,adiabatic}} = \sum_j x_{0,j}^2 \hat{q}_{\text{ji,diabatic}} \tag{12}$$

Here, $x_{0,j}$ is the j-th element of the ground state eigenvector 0 and i are the position indices of donors and acceptors (D, A, D)×4. Even in the femtosecond transient absorption microscopy, only a small percentage of the molecules in the order of less than 1 % is simultaneously excited to prevent photodamage, justifying the ground state charge distribution in this semi-empirical model.

Then the same procedure of adding additional Coulomb terms to the diagonal elements of all diabatic states except the neutral one as outlined in 4.3 are applied. Typically, this procedure is repeated 15 to 20 times until convergence of $\sum_i |q_{\text{i,adiabatic,n}} - q_{\text{i,adiabatic,n-1}}|$, with n and $n-1$ being the self-consistent steps, is achieved. The diagonalized ground state is used for calculating the embedding as even the very strong laser pulses used in femtosecond transient absorption microscopy are not expected to excite a majority of the population. In some cases, a mixing parameter $\beta \in (0,1]$ is necessary to prevent oscillating behavior. Then, the new charges are

$$q_{\text{i,adiabatic,n}} = \beta \tilde{q}_{\text{i,adiabatic,n}} + (1-\beta) q_{\text{i,adiabatic,n-1}} \tag{13}$$

with actually used charges q and the newly computed charges $\tilde{q}$.

The adiabatic embedding approach can be compared to a mean-field approach as the embedding is the same for all diabatic states and all of the charges are derived from a converged ground state calculation. In multiple simulation attempts, adiabatic embedding, although computationally more costly, gives the result that best matches the ellipsometry experiment [3] to the date of this publication.

4.5. Explicit treatment of multiple unit cells

Using reasonable limits for computational power, up to three unit cells can be calculated explicitly. This is done by adding the same monomers shifted by the lattice vectors. A $3 \times 1 \times 1$ unit cell results in a base of 531441 elements. In dense format, this would result

in more than $1\,\mathrm{TB}$ of memory requirements, therefore, sparse matrix algebra has to be employed. Using the sparse routines of CuPy, the calculation takes less than $30\,\mathrm{min}$ on a NVIDIA GeForce GTX 980 Ti and less than 45 minute by using SciPy's single core CPU routine on an AMD Ryzen 9 5950X.

4.6. Choice of monomers for OBC calculations

There are two goals which can be pursued by modifying which unit cell the four monomers are located in:

1. The symmetry of the system should be preserved as good as possible when compared to the periodic system

2. Explicitly treated chromophores should have the maximum amount of total interaction energy because embedding is always an approximation

The crystal information file of orthorhombic SQIB in [1] consists of the asymmetric unit of SQIB which is half a molecule. To generate the total unit cell, first the inversion transformation $\tilde{x} = -x$, $\tilde{y} = -y$, $\tilde{z} = -z$ is applied, followed by the three other unique transformations of space group 60 also defined in the crystal information file:

- $\tilde{x} = -x + \frac{1}{2}$, $\tilde{y} = -y + \frac{1}{2}$, $\tilde{z} = z + \frac{1}{2}$

- $\tilde{x} = -x$, $\tilde{y} = y$, $\tilde{z} = -z + \frac{1}{2}$

- $\tilde{x} = x + \frac{1}{2}$, $\tilde{y} = -y + \frac{1}{2}$, $\tilde{z} = -z$

First attempts were made by manually moving the chromophores to fit closer into the first unit cell, $\vec{a}$, $\vec{b}$ and $\vec{c}$ are the lattice vectors:

- Monomer 1 (centered in the unit cell): No change

- Monomer 2: $-\vec{c}$

- Monomer 3: $+\vec{a}$

- Monomer 4: $-\vec{a} + \vec{b} + \vec{c}$

This choice is physically justified because 1) it moves the monomers closer together, resulting in a higher intermolecular interaction and 2) the polarization symmetry determined by ellipsometry [3] is well-reproduced.

5. Results

All results are compared to the ellipsometry result in ref. [3], fig. 6. Unless explicitly stated, the parameters are always set to the following:

- $\eta = 0.737\,\mathrm{eV}$

(a) Original ESM charge geometry from symmetry operations

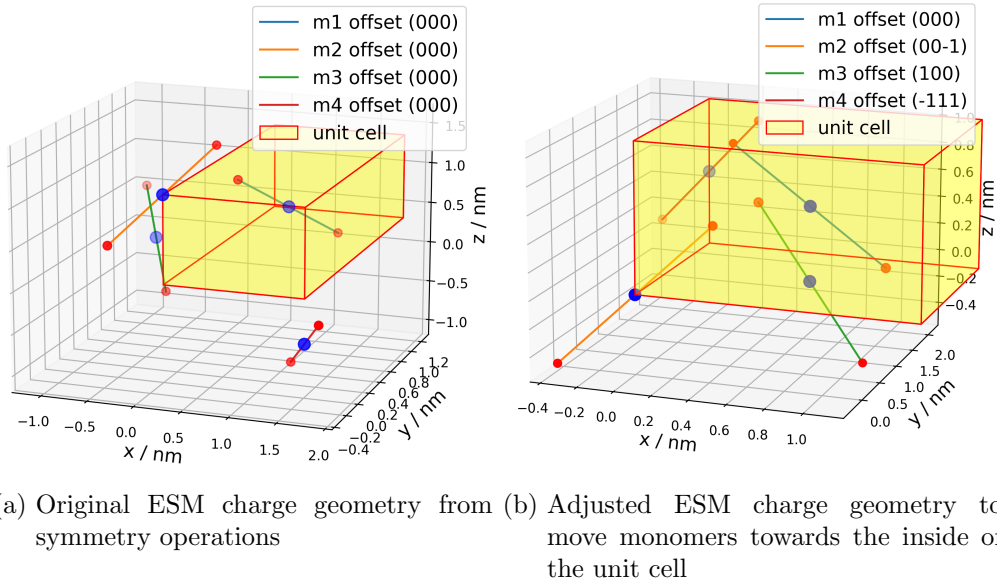(b) Adjusted ESM charge geometry to move monomers towards the inside of the unit cell

Figure 5: Charge centers used to model the D-A-D monomers in a unit cell. Crystal geometry from ref. [1], charges are placed on nitrogen atoms and in the center of the squaryllium moiety.

- $t = -1.05\,\text{eV}$

- $\epsilon_R = 2.0$

- $\sigma = 30\,\text{nm}$ in wavelength plots or $\sigma = 0.07\,\text{eV}$ in energy plots

- 5x5x5 supercell for embedding

- Convergence (12-20 steps) for adiabatic, self-consistent calculations

- $0.05\,\text{e}^2\text{nm}^2$ of lower cutoff for bright transitions

η and t are taken from a similar squaraine in ref. [7] and η is modified to match the one-photon transition at $653\,\text{nm}$ of $1\,\%$ SQIB mixed with PMMA, a similar sample to ref. [20]. With further 2PA measurements, there may be further adjustments to better replicate the experiment. The relative dielectric constant ϵ_R is set to 2.0 as it resulted in a relatively good match, but this will also be adjusted based on other experiments. For *bright* transitions, a physical cutoff is chosen in favor of a purely numerical one as the missing periodic boundary conditions and their approximation often account for a slight increase of otherwise dark transitions not present in the crystal.

Fig. 7 and 8 are results calculated using the DADMultimer code. Interestingly, the extended tetramer in fig. 8 shows inhomogeneous broadening which results on nearly overlapping transitions resulting in peak broadening. Also, it should be noted that the result is extensive with system size and not normalized to a unit cell, resulting in the

≈ 3-fold increase in oscillator strength. While the resulting spectrum looks valid, this approximation of the periodic system does not provide a better description than the open boundary condition tetramer due to the multitude of broadened peaks.
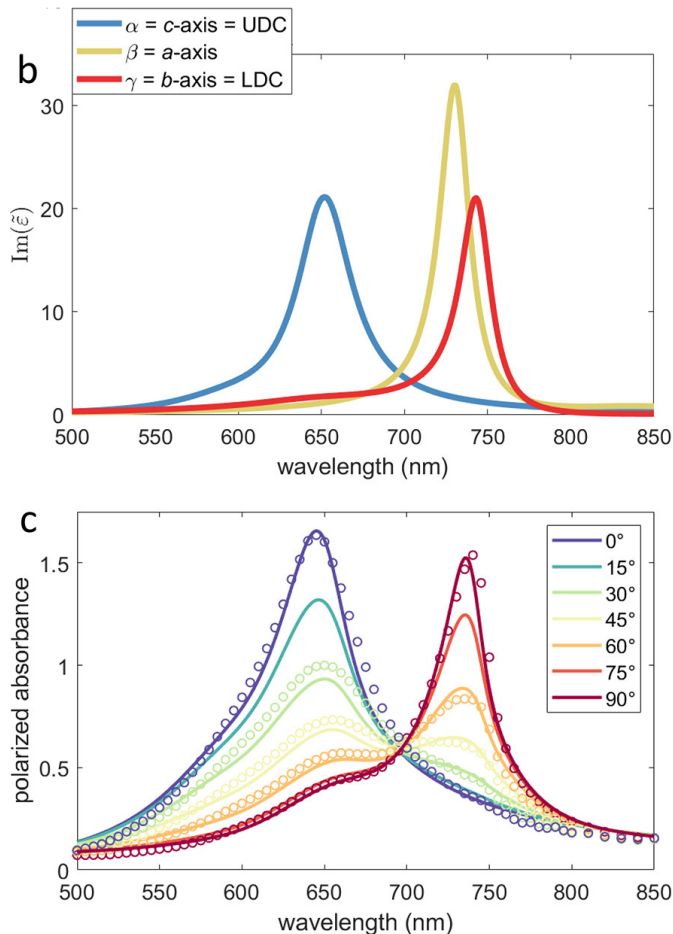

Figure 6: Experimentally determined states from Mueller Imaging Ellipsometry in ref [3]

The diabatic embedding result in fig. 9 looks like a compelling approximation of the experimental result at first glance. However, the peak positions do not match up with experiment very well and the embedding into a diabatic environment means that the diabatic states all experience different charges without coupling, making the result non-physical. As a result, the mean-field, adiabatic embedding approach is given preference.

In contrast, the adiabatic embedding surrounds each state with the same, self-consistently calculated electronic ground state charge distribution. Remarkably, the three bright states form a line which makes associating the peaks with experiment and linearly moving the dark state feasible (see the Jablonski diagram in fig. 3). This results in a dark state position of 1.79 eV or 692 nm. While, again, there is a clear difference between experimental positions and the result of the essential states model, this is a
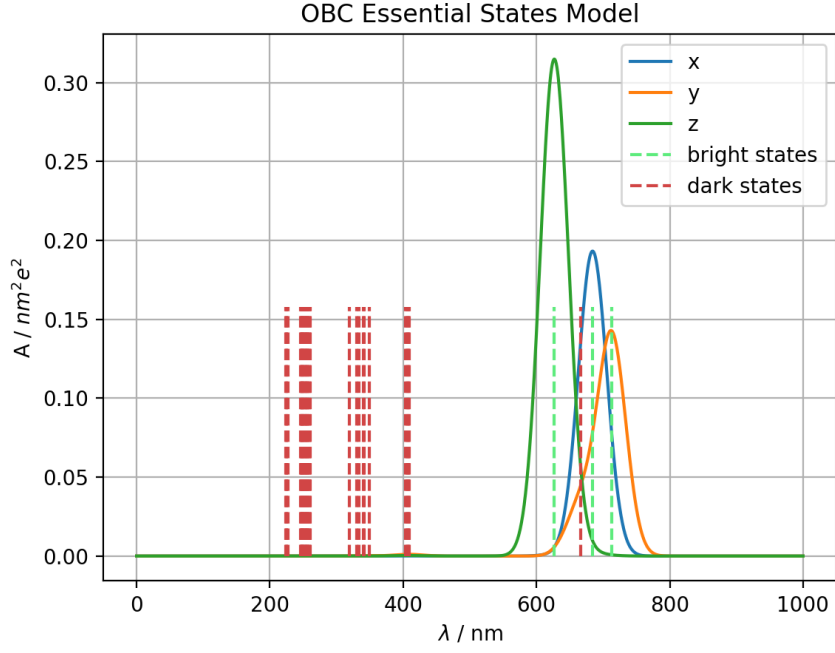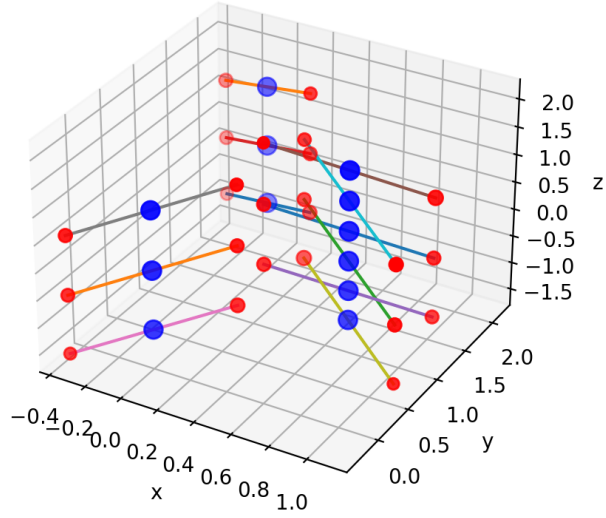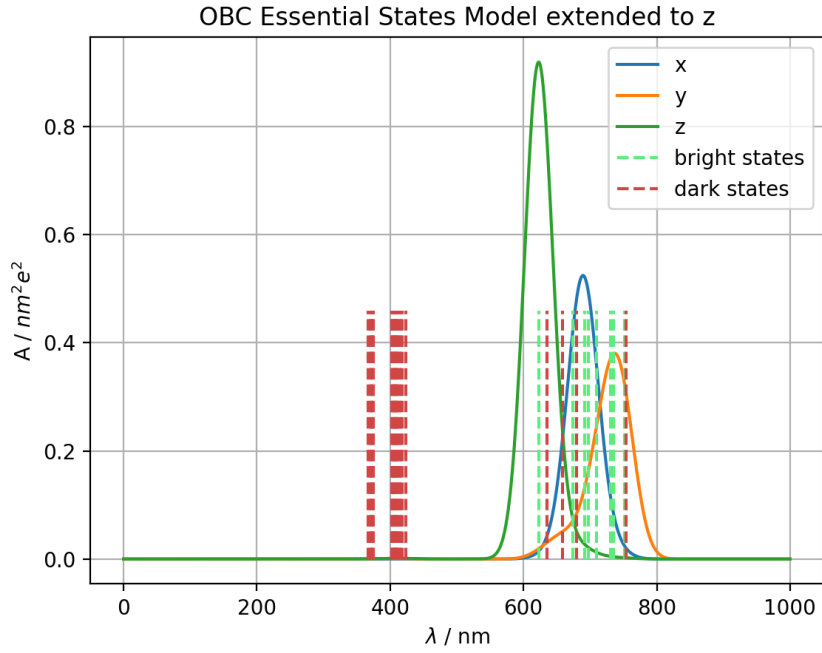
(a) Transitions and dark state positions
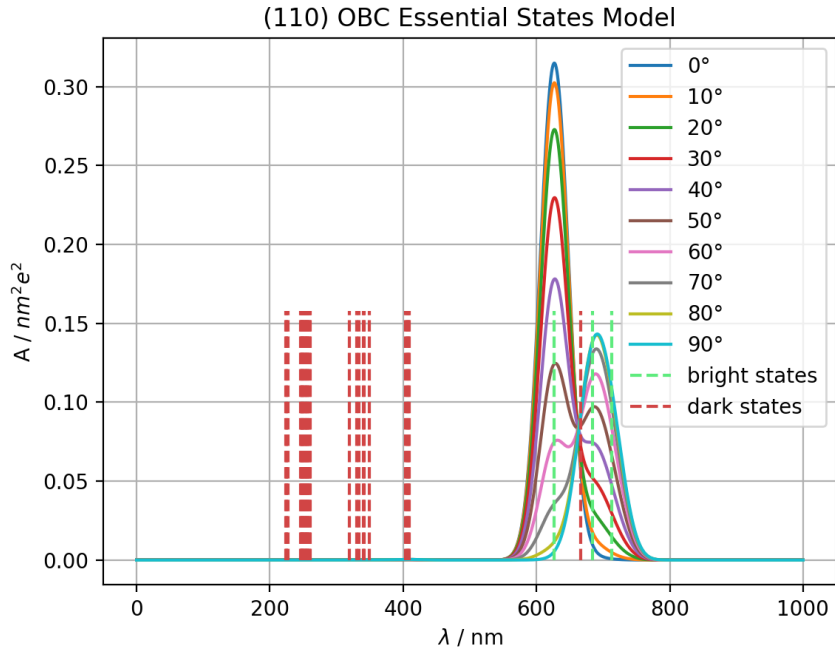
(b) Projected result onto the (110) plane

Figure 7: Tetramer in open boundary conditions, first 30 states calculated using Lanczos algorithm. Bright states appear at $1.74\,\text{eV}$, $1.81\,\text{eV}$, $1.86\,\text{eV}$ and $1.98\,\text{eV}$, the state at $1.86\,\text{eV}$ is below the chosen brightness cutoff of $0.05\,\text{eV}^2\text{nm}^2$ and only visible as a shoulder in the orange y curve.

(a) Geometry. Colors of the charge centers indicate sign (red positive, blue negative) and their size the magnitude of the resulting adiabatic charges.

(b) Transitions and dark state positions

Figure 8: Tetramer with two neighboring unit cells along the z axis. 30 states calculated using Lanczos algorithm. Bright states appear at $1.65\,\mathrm{eV}$, $1.69\,\mathrm{eV}$, $1.70\,\mathrm{eV}$, $1.75\,\mathrm{eV}$, $1.78\,\mathrm{eV}$, $1.79\,\mathrm{eV}$, $1.84\,\mathrm{eV}$ and $1.99\,\mathrm{eV}$ while the low dark states $1.64\,\mathrm{eV}$, $1.82\,\mathrm{eV}$, $1.88\,\mathrm{eV}$ and $1.95\,\mathrm{eV}$ are below the chosen cutoff.
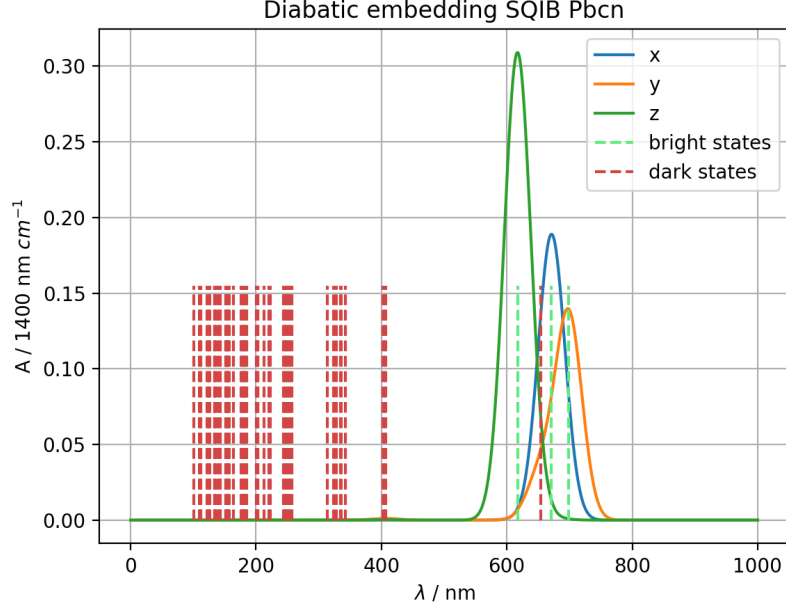
Figure 9: Diabatic embedding spectrum. Bright states appear at $1.77\,\mathrm{eV}$, $1.85\,\mathrm{eV}$ and $2.01\,\mathrm{eV}$ and a low dark state at $1.85\,\mathrm{eV}$.

more promising result and the description is qualitatively correct. The fit result is $E_{\mathrm{experiment}} = -0.43 + 1.38 * E_{\mathrm{ESM}}$, indicating that both the transition spacing and a constant offset are adjusted, the second of which can be attributed to a missing crystal shift occurring between open boundary conditions and periodic boundary conditions. This result most clearly resembles the close proximity of the states LDC1 and LDC2 in the experimental result [3] in fig. 6 and further improvements are expected by inserting an experimentally determined dielectric constant ϵ_R.
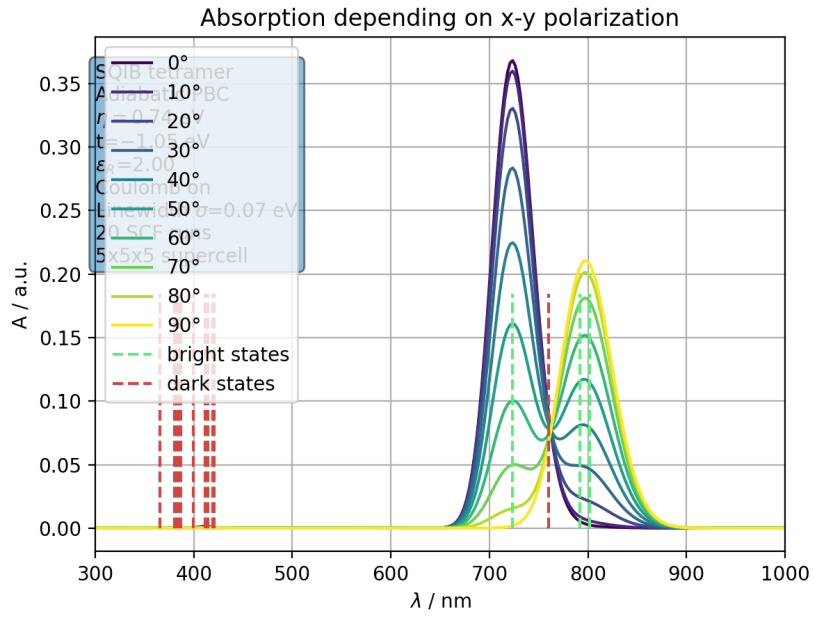
(a) Adiabatic embedding result projected onto the (110) plane.
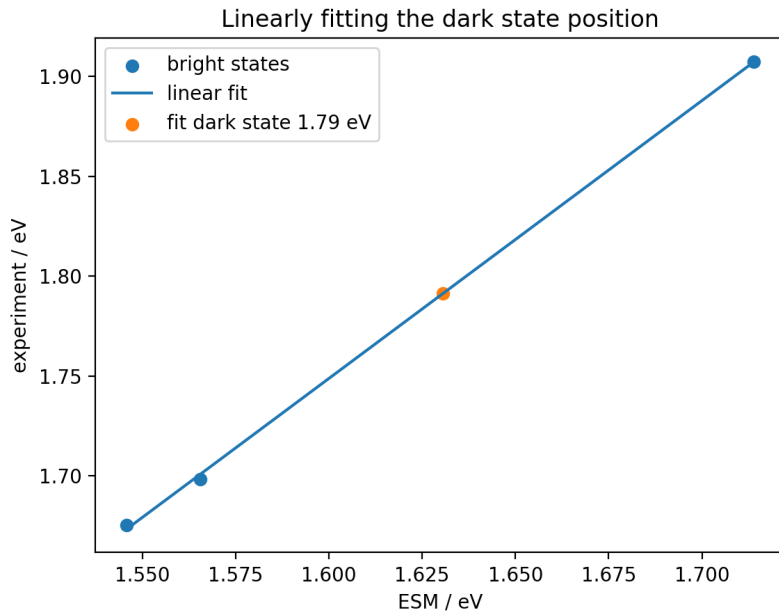
(b) Linear fit of the ESM dark state to the experimental results

Figure 10: Adiabatic embedding of the SQIB tetramer. Bright states appear at 1.55 eV, 1.57 eV and 1.71 eV, a dark state at 1.63 eV.

6. Summary and outlook

After initially porting the essential states model for D-A-D chromophores from Fortran 77 to Python 3.10, the system is extended to a tetramer with open boundary conditions. While this result already resembles the experimentally determined spectrum, further improvements are made by embedding the system in its adiabatic ground state which approximates the periodic crystal with Coulomb interactions with a mean-field, almost crystalline environment.

Further ideas to extend the essential state model in orthorhombic squaraine molecular crystals is to (1) implement adiabatic embedding in DADMultimer, allowing for the exchange of explicitly treated monomers and those in a mean field embedding, (2) the experimental determination of the dielectric constant at optical frequencies to improve the Coulomb interaction agreement and (3) the implementation of simulated two-photon absorption to determine further experiments.

It is planned to look for dark states which can not be directly excited using continuous wave (CW) light sources using transient absorption microscopy; in particular, this involves comparing dark states in the ultraviolet regions with essential state model simulations. It is expected that the essential states model results give insight into further experiments, leading to a more thorough understanding of the light-matter interaction of the squaraine system. In the farther future, there are also plans to calculate transition rates in order to simulate transient absorption delay scans.

7. Acknowledgements

A. Tetramer code documentation

This section describes the capabilities, functions and parameters used to calculate essential state model results in all of the classes. It also shows the inheritance structure for possible and realized extensions such as the embedding approaches.

A.1. Crystal Information File readout and JSON storage

As a well-established format readable by computers and humans alike, JSON is used to store cartesian charge center coordinates and the transform matrix. These properties are calculated from the Crystal Information File provided in the CCDC in entry 1567104 [1] using the PyCIFRW package [10]. Symmetry operations are then applied to the assymetric cell from the symmetry operations listed in this file, given by space group 60. From the lattice vectors and angles, the transform matrix is calculated according to ref. [2], theoretically allowing for the handling of non-orthogonal systems.

- x, y, z: Coordinates of the monomers in $(D_{1,1}, A_1, D_{2,1}, D_{1,2}, A_2, D_{2,2} \ldots)$ format

- M: Transform matrix for unit cells. $\vec{r}_{\text{cartesian}} = M \cdot \vec{r}_{crystal}$, lattice vectors $\vec{a}, \vec{b}$ and $\vec{c}$ are the columns of this matrix

A.2. SpectrumGenerator

Abstract base class for Hamiltonian problems including diagonalization, absorption spectrum calculation and plotting functions.

- Inherits ABC: Can not be used directly

- function diagonalizeH: Full diagonalization of the Hamiltonian matrix using `numpy.linalg.eigh`. By default, sets `self.eval` to the eigenvalues and `self.evec` to the corresponding eigenvectors.

- function calculateAbsorptionSpectrum: Abstract. Should calculate the absorption spectrum.

- function plotAbsorptionSpectrum: Abstract. Should plot the absorption spectrum in its most basic form.

The class is not very useful as most of the functions used by inherited classes go much beyond its capabilities, so it was not used for the later code DADMultimer.py.

A.3. DADTetramer

Main class for open boundary conditions calculations of D-A-D tetramers such as anilino squaraines. Starting from coordinates, energies η and t, a relative dielectric constant ϵ_R to take effective charge shielding into account, this class is capable of calculating the Hamiltonian of four aggregated monomers in the gas phase. Its forAll functions call

energy calculations and coupling functions for all relevant combinations of excitations, following a functional programmign paradigm. Unlike the newer class DADMultimer, this class uses dense matrices and is therefore limited by memory size, but calculates all of the possible excited states.

- Inherits SpectrumGenerator. Energies are in $1400 \, \mathrm{cm^{-1}}$ (1 assumed vibrational quanta) due to compatibility with the DAD dimer code of Prof. Spano (vibration is not considered in this code), distances are in nm.

- nnCT, tCT: η and t energies of the essential states model.

- epsilonR: Relative dielectric constant.

- x, y, z: Coordinates of the monomers in the same format as in the JSON file in sec. A.1

- ux, uy, uz: Dipole moments in the diabatic basis in $1400 \, \mathrm{nm \, cm^{-1}}$

- cf: Conversion factor $\frac{1}{4\pi\epsilon_0}$ for Coulomb interaction

- charges: $q_{\mathrm{D1}}, q_{\mathrm{A}}, q_{\mathrm{D2}} = [1, -1, 1]$ by default, for calculating Coulomb interactions.

- linewidth: σ in $A(E) = \sum_i \exp\left(-\frac{(E-E_i)^2}{\sigma^2}\right)$ for peak plotting

- setGeometry, setMonomerEnergy, setCouplingStrength, setLinewidth, setDielectricConstant: Wrappers for setting the corresponding variables directly (more readable)

- setGeometryFromJson: Using the format in sec. A.1, read self.x, self.y and self.z from the provided JSON filename.

- setDipoleMoment: Calculate diabatic dipole moments from coordinates and charges

- calculateCoulombTerm: combination is two indices of the interacting monomers (e.g. $[1, 3]$ would be monomers 2 and 4 in zero-based notation), chargePosition1 and chargePosition2 are $[0, 1]$ for $|Z_1\rangle$ states and $[1, 2]$ for $|Z_2\rangle$ states (relative indexing of charges and coordinate index.) Returns Coulomb term without multiplication of $\frac{1}{4\pi\epsilon}$.

- calculateDoubleCoulomb: doubleExcitation1 and doubleExcitation2 are 1 for $|Z_1\rangle$ and 2 for $|Z_2\rangle$ state, combination the same as in calculateCoulombTerm. Returns the Coulomb potential of the four interacting charge combinations.

- calculateTripleCoulomb: tripleExcitation1-3 are similar to calculateDoubleCoulomb, neutralPosition indicates the neutral index (neutralIndex= 1 means state [tripleExcitation1, 0, tripleExcitation2, tripleExcitation3].

- calculateQuadrupleCoulomb: Sums and returns the potential of all combinations of all four excited, diabatic monomers

- forAllSingles, forAllDoubles, forAllTriples, forAllQuadruples: Takes a function fcn and runs it for every possible combination of single, double, triple and quadruple excitations in the syntax of singleDiagonal to quadrupleDiagonal

- singleDiagonal, doubleDiagonal, tripleDiagonal, quadrupleDiagonal: Set the self.currentElement diagonal entry in self.H to $n*\eta+V_C$, n being the number of diabatically excited monomers, using the same syntax as calculateDoubleCoulomb and other Coulomb functions. Also set self.nes1-4 to the index of the current element to look up in the non-diagonal entries later on.

- coupleNeutralSingle, coupleSingleDouble, coupleDoubleTriple, coupleTripleQuadruple: Take a lower and a higher excited diabatic state and set the corresponding non-diagonal element to the Essential States Model energy t. Vibronic coupling would consider the Frank-Condon overlap here, but this was not done in this first version as it would increase the system size in this tetramer too much.

- Helper functions strSingle, strDouble, numTriple, numQuadruple, strTriple, strQuadruple: Convert a specific combination to a number or string, can help with determining if a combination of diabatic excitations is coupled or not

- compileTetraH: Main filling function for the Hamiltonian. Fills all of the upper diagonal elements of the Hamiltonian matrix self.H according to sec. 4.2.

- diagonalizeH: Same as in the base class SpectrumGenerator

- addSingleOs, addDoubleOs, addTripleOs, addQuadrupleOs: Calculate transition dipole moment oscillator strengths by doing a base transformation into the adiabatic base according to eq. (5)

- neutralU, singleU, doubleU, tripleU, quadrupleU: Returns the diabatic dipoles for the corresponding excitation in a tuple with the excitation index nes: [nes, ux, uy, uz]. This is done by summing up the diabatic dipole moments according to the combinations.

- calculateAllTdm: Returns a matrix with all transition dipole moments in the adiabatic base. The calculation is the same as in neutralU etc., but in a matrix form which can then be used for two-photon absorption codes.

- calculateAbsorptionSpectrum: self.energies, self.absX, self.absY and self.absZ are set to a range of energies and the corresponding sum of transition peaks.

- plotAbsorptionSpectrum: Use matplotlib.pyplot.subplots() to generate a figure axis combination and plot the simulation result. matplotlib.pyplot.show() can be used afterwards to show it. Most of the simulation results are plotted using external routines.

- projectOscillatorStrengths: Calculate the projection of the oscillator strengths self.osxx, self.osyy and self.oszz to the specified 3-d vector. Useful for plotting

the simulation result along non-cartesian coordinates, such as the in-plane directions of the experiment as outlined in sec. 2.

A typical calculation would initialize a default instance of DADTetramer() followed by setting all of the parameters, compileTetraH, diagonalizeH, calculateAbsorptionSpectrum and then either the integrated plotting routine or similar external routines.

A.4. DADTetramerEmbedded

Another abstract base class ABC, this includes reading the unit cell matrix M from JSON, the unit cell vectors a, b and c as variables and multiple cutoff to define the range of neighboring unit cells to include. It should be minded that, at the time of this publication, the code can only handle orthogonal systems, but minor changes to functions using self.a, self.b and self.c can change that.

- a, b, c: Lattice vectors in nm

- aRange, bRange, cRange: Range of unit cells to be considered in the calculation (e.g. [-2, 2] for a 5x5x5 supercell)

- setGeometryFromJson: Read lattice vectors as well as the underlying coordinates. They are assumed to be in Angstrom in the M matrix as per Crystal Information File standards.

- setUnitCell, setMultipleCutoff: Wrapper functions for a, b, c, aRange, bRange and cRange

A.5. DADTetramerDiabaticEmbedded

This class inherits DADTetramerEmbedded and extends some of its Coulomb calculation to include copies of the internal diabatic states in neighboring unit cells.

- selfInteraction: Calculate the Coulomb interaction between an excited monomer and its own copies; singleIndex is 0-based for the monomer and excitation is 1 for $|Z_1\rangle$ and 2 for $|Z_2\rangle$

- singleDiagonal, doubleDiagonal, tripleDiagonal, quadrupleDiagonal: These functions are overridden to automatically add Coulomb interaction to neighboring unit cells to all diagonal elements apart from the neutral state $|NNNN\rangle$

A.6. DADTetramerAdiabaticEmbedded

This class also inherits DADTetramerEmbedded, but instead of using the diabatic state copied to neighboring unit cells, the adiabatic ground state charges are calculated according to eq. (12) in a self-consistent manner.

- mixingBeta: Mix new and old charge distributions according to eq. (13)

- referenceState: In theory, it would be possible to perform adiabatic embedding in excited charge distributions. However, even in transient absorption experiments, only a minority of monomers is excited according to transient absorption experiments, so using the ground state referenceState = 0 is justified.

- calculateChargeMatrix: Calculate all charges in the diabatic basis $q_{\text{diabatic},i,j}$ with i the diabatic state index and j the charge center's coordinate index. Return this matrix.

- embeddingStep: Compile tetramer Hamiltonian, diagonalize it, calculate charges using calculateChargeMatrix, transform them into the adiabatic base using matrix multiplication: $\hat{q}_{\text{adiabatic}} = \vec{x}_0 \cdot \hat{q}_{\text{diabatic}}$, set self.embeddingCharge to the result. If this was already done at least once, the calculation is already performed using the mean-field embedding approach.

- addSingleEmbeddedCoulomb: Calculate interaction between excited monomer given by singleIndex (monomer index 0-3) and excitation (1 $|Z_1\rangle$, 2 $|Z_2\rangle$)

- singleDiagonal, doubleDiagonal, tripleDiagonal, quadrupleDiagonal: Are overridden to include Coulomb terms with the neighboring unit cells

The workflow here changes from DADTetramer as adiabatic embedding is a self-consistent process typically necessitating 12-20 cycles to achieve sufficient convergence. A possible convergence criterion is to check the value of $\sum_i |q_{i,n} - q_{i,n-1}|$ with charge index i and self-consistent iteration n. Results lower than 1×10^{-4} unit charges e typically do not change the spectrum and are sufficient due to the broad line widths involved. One starts to set all parameters and then repeatedly calls embeddingStep, then proceeds with calculateAbsorptionSpectrum as in DADTetramer.

A.7. DADMultimer and DADMonomer

At the time of this publication, the code in DADMultimer handles an arbitrary size of D-A-D monomers in open boundary conditions. To facilitate larger systems, the Hamiltonian matrix is stored in SciPy's dok_array format, that is, its non-zero entries are stored in a dictionary of keys. The code is also separated into two different classes, DADMultimer and DADMonomer, where the latter class handles coordinates and charges, can return charge centers based on diabatic excited state $|Z_1\rangle$ or $|Z_2\rangle$ and calculate its own interaction energy with another monomer and its dipole moment. In DADMultimer, the aggregation itself is handled including the setup of the sparse Hamiltonian, CPU and GPU-based sparse diagonalization and charge calculation as in the adiabatic embedding class. All energies are in eV, all distances in nm.

DADMultimer class

- monomers: List of DADMonomer involved in the aggregation

- monomer_energy, interaction_energy: η and t in the essential states model, respectively

- coulomb_factor: $\frac{1}{4\pi\epsilon_0}$ in the unit system

- hamiltonian: Sparse Hamiltonian matrix

- transform_matrix: Transform matrix from crystal to cartesian coordinates

- eigenvalues, eigenvectors: Result of the diagonalization

- all_excitations: Dictionary of excitations. Keys are, for example, [2, 1, 0, 1].to-bytes(), values are a tuple of (excitation index, [2, 1, 0, 1]). This is used instead of the n-dimensional arrays in DADTetramer to accommodate arbitrary lengths.

- load_coordinates_from_json: Read coordinates and transform matrix in the JSON format explained in sec. A.3

- copy_along_unit_cell: Extend the system to cover multiple unit cells explicitly. For a tetramer, three unit cells is a useful restriction to limit memory and computing requirements.

- set_all_epsilon_R: Since the relative dielectric constant is needed for Coulomb interactions in the DADMonomers, this is a convenient way to set it for all of the monomers.

- compile_multi_hamiltonian: Allocate the sparse Hamiltonian matrix, set all diagonal elements including diabatic monomer energy and Coulomb interaction and the coupling, non-diagonal terms. Since sparse diagonalization routines are based on matrix multiplication, the resulting, symmetric Hamiltonian matrix is stored in full.

- for_all_excitations_degree: Uses SymPy's multiset_permutations routine to run functions for all diabatic states with the given number of excited monomers in degree. max_excitations can be used to limit the total number of excitations for approximations. All *args are treated as functions and run with one argument, an array of monomer excitations, e.g. [2, 1, 0, 1].

- diagonalize_sparse(_gpu): Use SciPy's or CuPy's sparse eigsh routine to calculate a number k of lowest eigenvalues and associated eigenvectors. If using the GPU, it must be possible to locate a valid CUDA environment using CUDA_PATH (CUDA main directory) and LD_LIBRARY_PATH (CUDA math libraries and CUDA libraries) as CuPy is only imported within the diagonalization routine.

- calculate_summed_dipole_moments: Sum the individual dipole moments of all monomers for a given diabatic state, e.g. [2, 1, 0, 1].

- calculate_charges: Returns an array of DADMonomers with charges calculated from the reference eigenvector, per default the ground state 0. This is useful for plotting the geometry and will be used for adiabatic embedding in the future.

While, currently, the arbitrary addition of additional monomers to improve the periodicity approximation has not yielded any success, it is planned to combine it with adiabatic embedding, covering the most interacting monomers in the unit cell while treating its environment in the mean-field manner described in sec. 4.4.

DADMonomer class

- coordinates: Coordinate matrix. charges[0] would be [x, y, z] of D_1, charges[1] of A.

- charges: Charge vector in $[q_{D1}, q_A, q_{D2}]$ format. In the diabatic basis, these are assumed to be [1, -1, 1], but inherited classes could use this for adiabatic embedding calculations.

- load_from_dict, get_dict: Loading from and saving to dictionary (useful for JSON exports and imports)

- get_excited_coordinates: returns a tuple with coordinates associated with charge centers depending on the input state (diabatic states are, strictly speaking, not physical excitations)

- get_excited_charges: returns a tuple with charges depending on the diabatic input state

- calculate_coulomb_interaction: returns the interaction energy of this monomer with another DADMonomer depending on its own and the other diabatic states

- calculate_dipole_moment: return the dipole moment $\sum_i q_i * \vec{r}_i$ with the reference point in the middle of both charges

References

[1] Frank Balzer et al. "Spotlight on Excitonic Coupling in Polymorphic and Textured Anilino Squaraine Thin Films". In: *Crystal Growth & Design* 17.12 (2017), pp. 6455–6466. DOI: 10.1021/acs.cgd.7b01131. eprint: https://doi.org/10.1021/acs.cgd.7b01131. URL: https://doi.org/10.1021/acs.cgd.7b01131.

[2] *Coordinate system transformation.* URL: https://www.ruppweb.org/Xray/tutorial/Coordinate%20system%20transformation.htm.

[3] Sebastian Funke et al. "Determining the Dielectric Tensor of Microtextured Organic Thin Films by Imaging Mueller Matrix Ellipsometry". In: *The Journal of Physical Chemistry Letters* 12.12 (2021). PMID: 33739845, pp. 3053–3058. DOI: 10.1021/acs.jpclett.1c00317. eprint: https://doi.org/10.1021/acs.jpclett.1c00317. URL: https://doi.org/10.1021/acs.jpclett.1c00317.

[4] Charles R. Harris et al. "Array programming with NumPy". In: *Nature* 585.7825 (Sept. 2020), pp. 357–362. DOI: `10.1038/s41586-020-2649-2`. URL: `https://doi.org/10.1038/s41586-020-2649-2`.

[5] Pascal Heim. "Femtosecond Light-Matter Interaction Processes from Isolated Molecules to Molecular Crystals". Graz University of Technology, 2022.

[6] Nicholas J. Hestand and Frank C. Spano. "Expanded Theory of H- and J-Molecular Aggregates: The Effects of Vibronic Coupling and Intermolecular Charge Transfer". In: *Chemical Reviews* 118.15 (Apr. 2018), pp. 7069–7163. DOI: `10.1021/acs.chemrev.7b00581`. URL: `https://doi.org/10.1021/acs.chemrev.7b00581`.

[7] Nicholas J. Hestand et al. "Correction to "Confirmation of the Origins of Panchromatic Spectra in Squaraine Thin Films Targeted for Organic Photovoltaic Devices"". In: *The Journal of Physical Chemistry C* 126.27 (June 2022), pp. 11436–11437. DOI: `10.1021/acs.jpcc.2c04087`. URL: `https://doi.org/10.1021/acs.jpcc.2c04087`.

[8] Aaron Meurer et al. "SymPy: symbolic computing in Python". In: *PeerJ Computer Science* 3 (Jan. 2017), e103. ISSN: 2376-5992. DOI: `10.7717/peerj-cs.103`. URL: `https://doi.org/10.7717/peerj-cs.103`.

[9] Ryosuke Okuta et al. "CuPy: A NumPy-Compatible Library for NVIDIA GPU Calculations". In: *Proceedings of Workshop on Machine Learning Systems (LearningSys) in The Thirty-first Annual Conference on Neural Information Processing Systems (NIPS)*. 2017. URL: `http://learningsys.org/nips17/assets/papers/paper_16.pdf`.

[10] *PyCifRW 4.4.5 on PyPI - Libraries.io*. URL: `https://libraries.io/pypi/PyCifRW`.

[11] Guido Van Rossum and Fred L. Drake. *The Python Language Reference — Python 3.11.5 documentation*. URL: `https://docs.python.org/3/reference/index.html`.

[12] Robert Schwarzl. "Femtosecond Transient Absorption Microscopy of Textured Anilino Squaraine Thin Films to Investigate Population Dynamics of Davydov States". Graz University of Technology, 2021.

[13] Robert Schwarzl et al. "Transient absorption microscopy setup with multi-ten-kilohertz shot-to-shot subtraction and discrete Fourier analysis". In: *Optics Express* 30.19 (Sept. 2022), p. 34385. DOI: `10.1364/oe.466272`. URL: `https://doi.org/10.1364/oe.466272`.

[14] K. M. Shafeekh et al. "Asymmetric Squaraine Dyes: Spectroscopic and Theoretical Investigation". In: *The Journal of Physical Chemistry B* 117.28 (2013). PMID: 23777344, pp. 8536–8546. DOI: `10.1021/jp401099g`. eprint: `https://doi.org/10.1021/jp401099g`. URL: `https://doi.org/10.1021/jp401099g`.

[15] Francesca Terenziani et al. "Charge Instability in Quadrupolar Chromophores: Symmetry Breaking and Solvatochromism". In: *Journal of the American Chemical Society* 128.49 (2006). PMID: 17147384, pp. 15742–15755. DOI: 10.1021/ja064521j. eprint: https://doi.org/10.1021/ja064521j. URL: https://doi.org/10.1021/ja064521j.

[16] Francesca Terenziani et al. "Charge Instability in Quadrupolar Chromophores: Symmetry Breaking and Solvatochromism". In: *Journal of the American Chemical Society* 128.49 (Nov. 2006), pp. 15742–15755. DOI: 10.1021/ja064521j. URL: https://doi.org/10.1021/ja064521j.

[17] Francesca Terenziani et al. "Essential-State Model for Polymethine Dyes: Symmetry Breaking and Optical Spectra". In: *The Journal of Physical Chemistry Letters* 1.12 (2010), pp. 1800–1804. DOI: 10.1021/jz100430x. eprint: https://doi.org/10.1021/jz100430x. URL: https://doi.org/10.1021/jz100430x.

[18] Andrei Tokmakoff. *Time-Dependent Quantum Mechanics and Spectroscopy – Notes*. 2014. URL: https://tdqms.uchicago.edu/.

[19] Pauli Virtanen et al. "SciPy 1.0: Fundamental Algorithms for Scientific Computing in Python". In: *Nature Methods* 17 (2020), pp. 261–272. DOI: 10.1038/s41592-019-0686-2.

[20] Chenyu Zheng et al. "Measurement and Theoretical Interpretation of Exciton Diffusion as a Function of Intermolecular Separation for Squaraines Targeted for Bulk Heterojunction Solar Cells". In: *Journal of Physical Chemistry C* 124 (7 Feb. 2020), pp. 4032–4043. ISSN: 19327455. DOI: 10.1021/acs.jpcc.9b11816. URL: https://dx.doi.org/10.1021/acs.jpcc.9b11816.

[21] Chuwei Zhong et al. "Davydov Splitting in Squaraine Dimers". In: *The Journal of Physical Chemistry C* 123.30 (July 2019), pp. 18734–18745. DOI: 10.1021/acs.jpcc.9b05297. URL: https://doi.org/10.1021/acs.jpcc.9b05297.

[22] Yifan Zhu and Ji Xin Cheng. *Transient absorption microscopy: Technological innovations and applications in materials science and life science*. Jan. 2020. DOI: 10.1063/1.5129123. URL: https://doi.org/10.1063/1.5129123.